100 Gbps Indoor Access and 4.8 Gbps Outdoor Point-to-Point LiFi Transmission Systems Using Laser-Based Light Sources

Cheng Chen, Sovan Das, *Member, IEEE*, Stefan Videv, Adrian Sparks, Sina Babadi, Aravindh Krishnamoorthy, *Graduate Student Member, IEEE*, Changmin Lee, Daniel Grieder, Kathleen Hartnett, Paul Rudy, James Raring, Marzieh Najafi, *Member, IEEE*, Vasilis K. Papanikolaou, *Member, IEEE*, Robert Schober, *Fellow, IEEE*, and Harald Haas, *Fellow, IEEE*

(Invited Paper)

***Abstract*—In this paper, we demonstrate the communication capabilities of light-fidelity (LiFi) systems based on high-brightness and high-bandwidth integrated laser-based sources in a surface mount device (SMD) packaging platform. The laser-based source is able to deliver 450 lumens of white light illumination and the resultant light brightness is over 1000 $\mathrm{cd/mm^2}$. It is demonstrated that a wavelength division multiplexing (WDM) LiFi system with ten parallel channels is able to deliver over 100 Gbps data rate with the assistance of Volterra filter-based nonlinear equalisers. In addition, an aggregated transmission data rate of 4.8 Gbps has been achieved over a link distance of 500 m with the same type of SMD light source. This work demonstrates the scalability of LiFi systems that employ laser-based light sources, particularly in their capacity to enable high-speed short range, as well as long-range data transmission.**

***Index Terms*—Laser diode, light-fidelity, optical wireless communication, surface mounting device, wavelength division multiplexing.**

I. Introduction

LASERS have been widely adopted and have been consistently used to develop new technologies in many fields, such as telecommunications, remote sensing and chemistry [2], [3]. In recent decades, visible light laser diodes (LDs) using Gallium nitride (GaN) material have been developed and have enabled several useful applications such as blue ray disc and high quality projection display systems [4], [5]. Recently, GaN-based LDs have been developed for solid state lighting (SSL) applications [6]. With the excellent energy-efficiency, GaN-based light-emitting diode (LED) lamps and light bulbs have been widely commercialised to replace the old incandescent lighting infrastructure. Compared to GaN-based LED illumination capabilities, GaN-based LDs can offer more than ten times higher brightness, longer lighting range, improved directionality and compact device dimension, which makes them suitable for scenarios where it is challenging for GaN-based LEDs to achieve the desired performance. Several potential applications of GaN-based LDs include virtual reality (VR)/augmented reality (AR) display, automotive lighting and advanced medical devices [7], [8].

In recent years, the concept of using light for wireless networking, light fidelity (LiFi), has been extensively investigated in both academia and industry [9]. A major advantage of this technology is that the infrastructure can provide both illumination and wireless communication functionalities concurrently. Millimeter-wave (mmWave), sub-terahertz (Sub-THz) and LiFi are potential technologies for future 6th generation (6G) wireless communication networks to deliver very high data rate and secure wireless transmission [10], [11]. These technologies have many similarities and different features, which are summarised in Table I. Most existing Sub-THz devices use electronic/photonic approaches with frequency conversion along with amplification components [12]. Due to the low conversion efficiency, the output power is generally in the range of less than 1 mW to a few mW. In contrast, many mmWave and optical frontend devices are available at low cost. The output power of these devices is in the range from a few mW to hundreds of mW. It is well-known that high-frequency wireless transmissions experience very high path loss [13]. Consequently, propagation directionality is important for the three

Manuscript received 30 November 2023; revised 27 March 2024; accepted 3 May 2024. Date of publication 13 May 2024; date of current version 27 June 2024. The work of Cheng Chen, Stefan Videv, Adrian Sparks, Sina Babadi, and Harald Haas was supported in part by Kyocera SLD Laser, in part by the Department of Science, Innovation & Technology in the U.K. through the Project: Enabling Architectures and Solutions for Open Networks (REASON), and in part by Engineering and Physical Sciences Research Council (EPSRC) under Grant EP/R007101/2 (Towards 100 Gigabit Wireless Networking by Light (Go-by-Light) (Ext.)) and Grant EP/X04047X/1 (Platform Driving The Ultimate Connectivity). The work of Harald Haas was also supported by Alexander von Humboldt Foundation in Germany for a research award. This is an invited paper which expands our ECOC 2023 invited talk and paper [DOI: 10.1049/icp.2023.2639] *(Corresponding author: Cheng Chen.)*.

Cheng Chen, Stefan Videv, Adrian Sparks, Sina Babadi, and Harald Haas are with the Department of Engineering, Cambridge University, CB3 0FA Cambridge, U.K (e-mail: cc2267@cam.ac.uk).

Sovan Das, Changmin Lee, Daniel Grieder, Kathleen Hartnett, Paul Rudy, and James Raring are with the Kyocera SLD Laser, Inc., Goleta, CA 93117 USA.

Aravindh Krishnamoorthy, Marzieh Najafi, Vasilis K. Papanikolaou, and Robert Schober are with the Institute for Digital Communications, Friedrich-Alexander-Universität Erlangen-Nürnberg, 91054 Erlangen, Germany.

Color versions of one or more figures in this article are available at https://doi.org/10.1109/JLT.2024.3400192.

Digital Object Identifier 10.1109/JLT.2024.3400192

TABLE I
A COMPARISON BETWEEN MMWAVE & SUB-THZ AND LIFI TECHNOLOGIES

Characteristics	mmWave	Sub-THz	LiFi
Front-end devices	Low complexity & medium to high output power	High complexity & low output power	Low complexity & medium to high output power
Directionality	Depends on No. of antennas, more divergent	Depends on No. of antennas, more divergent	Highly collimated
System complexity	High with a large No. of antennas	High with a large No. of antennas	Low
Spectrum regulation	Partially regulated	Partially regulated	Licence-free
Atmospheric effects	Sensitive to oxygen absorption/scattering, foliage, rain	Sensitive to water & oxygen absorption & scattering, rain, haze	Sensitive to fog, haze and scintillation effects
Eye safety optical/ RF output limits	Relaxed	Relaxed	Strict
Blockage/shadowing	Severely attenuated	Severely attenuated	Not penetrable through opaque objects
Achievable data rate	Very high data rate	Very high data rate	Very high data rate
Multi-path effects	Minor	Negligible	Negligible

technologies. Transmitting mmWave and Sub-THz signals directionally requires a large number of antennas and beamforming, but the resultant beam is generally more divergent than optical beams due to the greater diffraction-limited beam divergence angle and hardware restrictions. In contrast, highly directional optical beams can be achieved with a single optical source and simple optics, but beam steering techniques require further research and development. Regarding the system complexity, mmWave and Sub-THz communication systems are more complex owing to the need for multiple-input multiple-output (MIMO) techniques with a large number of antennas, radio frequency (RF) chains and phase shifters with intensive signal processing, while high-performance LiFi systems can be achieved with fewer components and much simpler designs. Considering the spectrum regulations, parts of the mmWave and Sub-THz spectrum are regulated for other applications, such as scientific sensing [14], while optical spectrum is currently licence-free. In the case of outdoor applications, mmWave, Sub-THz and optical signals are affected by various atmospheric effects, such as absorption and scattering due to small molecules in the air [14], [15]. These signals are also sensitive to various weather conditions, such as rain, fog and haze. Generally, the impacts of atmospheric effects on optical signals are more significant. In addition, optical signals experience scintillation effects, while the Sub-THz signal is immune to it. Nevertheless, the impact of atmospheric and scintillation effects in outdoor LiFi systems can be mitigated by using advanced optical and signal processing techniques. Regarding the output power limits, laser-based LiFi systems have restrictions for eye-safety reasons [16], while the emission of mmWave and Sub-THz signals have more relaxed output power restrictions. However, appropriate optical designs can avoid any eye safety hazards and minimise the risks of exceeding maximum exposure limits. Apart from the above differences, the three technologies have some similarities. The mmWave, Sub-THz and optical signals are vulnerable to link blockage. When blockage/shadowing happens, the link is either severely attenuated or completely interrupted. All three types of systems can achieve multi-GHz bandwidth and tens to hundreds of Gbps transmission data rates. Furthermore, due to the line-of-sight (LOS)-dominant propagation, all three systems experience minor/negligible multipath effects. Therefore, LiFi has been considered to be a promising candidate for 6G networks [17].

Most of the existing LiFi studies are based on LEDs, which pose limited modulation bandwidths in the range of a few to tens of MHz [18]. This significantly limits the achievable rate of LiFi systems. With research efforts focusing on how to extend the bandwidth of light sources, GaN-based micro LEDs and superluminescent diodes (SLDs) have been developed to deliver wireless data rates of over 10 Gbps [19], [20]. Despite the transmission rate improvement, micro LEDs can emit a very low optical power, which makes it difficult to provide effective illumination and long-range transmission. Therefore, laser-based light sources have been proposed for LiFi transmission [21]. LDs can provide dramatically improved brightness and a higher modulation bandwidth of more than 1 GHz compared to LEDs. These features make it possible to develop LiFi systems that can provide both high-brightness illumination and ultra-high speed/long-range data transmission.

There are several studies in the literature reporting results of LiFi research based on laser sources. GaN-based LDs with phosphor have been considered to achieve wireless transmissions with high data rates of a few Gbps using on-off keying (OOK) modulation [22], [23] and orthogonal frequency division multiplexing (OFDM) [24], [25]. A recent study considered using a free-form multipath lens to make laser-based LiFi transmission fulfil the eye-safety constraint [26], which is able to deliver a transmission data rate of over 1 Gbps and a high optical power output at the same time. The use of red-green-blue (RGB) lasers to establish white light illumination has been considered in [27], which also utilises the differences in wavelength to form wavelength division multiplexing (WDM) transmission so that the aggregated data rate can be improved. Our previous work has demonstrated the use of a dual LD unit with a surface mount device (SMD) package to develop a two-channel WDM LiFi system achieving a data rate of 26 Gbps with OFDM and high brightness white light illumination [28]. Recently, we have reported a ten channel WDM LiFi system with the improved version of the SMD laser sources in [1]. In this paper, we extend the work in [1] by including additional technical results, insights and discussions. By combining the data rates achieved by SMD

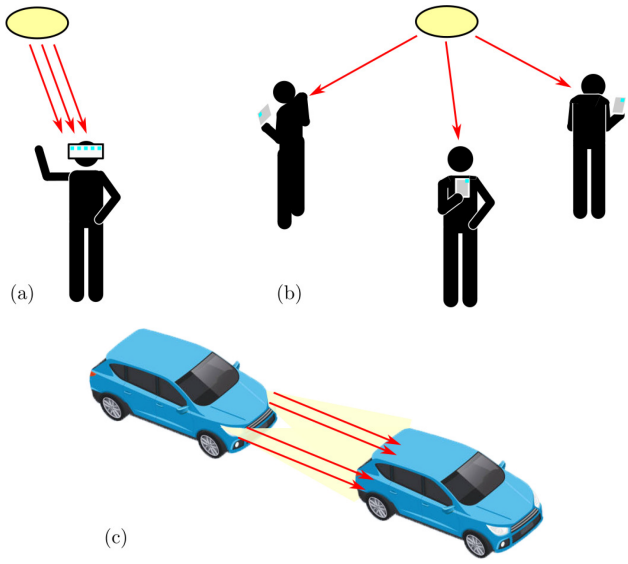

Fig. 1. High-speed and long-range LiFi use cases: (a) Indoor point-to-point links. (b) Indoor point to multi-points links. (c) Outdoor vehicle-to-vehicle links.

laser sources with ten wavelengths (including blue and infrared), an aggregate data rate of over 100 Gbps can be achieved. In addition, with the overlapped coverage of multiple SMD laser sources, the overall illumination range and brightness can be enhanced. Furthermore, we showcase a LiFi transmission based on the SMD laser light source in an outdoor environment with a link distance of 500 m, which achieved an aggregated data rate of 4.84 Gbps.

The remainder of this paper is structured as follows: The potential use cases of the demonstrated LiFi system is discussed in Section II. The schematic and design of the dual LDs SMD package is introduced in Section III. The LiFi system based on OFDM and nonlinear equaliser with a single channel is presented in Section IV. The 100 Gbps LiFi system with ten WDM channels are presented in Section V. The multi-Gbps data rate 500 m LiFi system is presented in Section VI. Finally, the conclusion is drawn in Section VII.

II. Use Cases of the Considered LiFi Systems

In this section, The potential use cases of the considered LiFi systems are discussed. In addition, the characteristics of LiFi, mmWave and Sub-THz technologies in these use cases are compared. In the indoor scenarios, there are many wireless link use cases where ultra-high data rate is required. For example, the future VR will offer a life-like immersive experience, where the image resolution will be in the range of 8 K to 12 K [29]. With the signal processing moving to the mobile edge, the required data rate will increase to tens of/hundreds of Gbps. In this case, the point-to-point high-speed LiFi parallel transmission can be used to fulfil the requirement, as shown in Fig. 1(a). Another useful point-to-point use case is where large files need to be transferred between two mobile devices. The high data rate wireless technology, such as LiFi, is able to significantly shorten the transmission time to a few seconds. Additionally, the transmission is secure and wireless. In these use cases, mmWave and Sub-THz communication systems can use their LOS MIMO features to achieve spatial multiplexing, which can significantly boost the achievable data rate. With VR applications, the beam forming capability can adapt the link with the motions of the headset, but fast channel estimation and beam adjustment pose additional challenges. LiFi systems can achieve parallel transmissions with fewer components and simpler approaches, such as WDM or multiple collimated beams carrying several data streams.

Providing high-speed wireless broadband to a large number of mobile users is an important use case for point-to-multi-point scenarios, as shown in Fig. 1(b). This is motivated by the extremely short reuse distance of LiFi as the light sources are directional and causes very little interferences to nearby users [30]. In conjunction with the wide bandwidth of the laser source, a very high data density can be achieved in this use case. High speed wireless point-to-multi-point links in Industrial 4.0 is another use case for the considered LiFi system, especially in factories where RF transmission is highly restricted. In these point-to-multi-point use cases, exploiting the large numbers of available antennas for beamforming, mmWave and Sub-THz communication systems can use multi-user (MU)-MIMO to serve multiple users simultaneously with high-speed transmissions. However, this necessitates sophisticated hardware and signal processing requirements. In contrast, presently, LiFi systems serve multiple users with a greater coverage area but need to share transmission resources among multiple users. Alternatively, multi-beam systems can be developed to serve users in a spatial division multiple access (SDMA) fashion. Further research on multi-user LiFi systems is of high interest.

The multi-Gbps long-range transmission capability of the laser-based LiFi will be useful in the outdoor vehicle-to-vehicle data transmission, as shown in Fig. 1(c). In recent years, laser-based headlights have been developed for automotive applications, which provide a great platform for deploying the demonstrated LiFi system to establish high-speed data transmission between vehicles for future Internet-of-Vehicle (IoV) and Intelligent transportation system (ITS) [31]. Last mile wireless backhaul links for wireless networks and wireless fronthaul links for distributed antenna systems are potential use cases of long-range LiFi systems, as well. In these outdoor long-range use cases, mmWave and Sub-THz systems are less affected by atmospheric effects such as attenuation and scintillation. However, the low transmitted power and more divergent beam limit the maximum propagation range of mmWave and Sub-THz systems and increase inter-user interference. In addition, the coherence bandwidth reduces with increasing link distance. Furthermore, the use of mmWave and Sub-THz communication may have restrictions due to spectrum regulations. In contrast, the LiFi spectrum is unregulated and LiFi systems can be easily integrated into existing lighting solutions such as vehicular lights. The high output optical power and better beam collimation can extend the link range to several km.

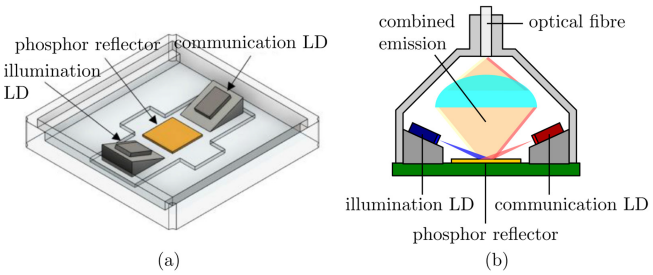

Fig. 2. (a) Schematic of the SMD light source with two LDs operating for illumination and communication functionalities. (b) Cross-section schematic of the SMD package.

III. Dual Wavelength Laser Integrated Surface Mounting Device

In this section, the design of the SMD laser source is introduced. The structure of the device package is similar to that presented in [28]. Two LDs are deployed on the two wedges mounted on the edges of the package and a phosphor reflector is deployed in the centre of the package, as shown in Fig. 2(a). The orientations of the LDs are configured so that the emitted collimated light incident to the phosphor reflector and the reflected light is coupled into an optical fibre, as shown in Fig. 2(b). One of the LDs emitting blue light (450 nm) is designed for illumination purposes. When the blue light incident to the phosphor reflector, part of the blue light is diffusely reflected, and part of the light excites the phosphor material to emit yellow light. The combination of blue and yellow light forms the white emission for illumination, which uses the same principle of the white LED for lighting [18]. Note that the phosphor reflector not only diffuses the collimated light from LDs but also converts the coherent light to non-coherent light, which is important for eye-safety considerations and illumination performance. The second LD emitting light of a different wavelength is designed for communication purposes. In order to establish a system with multiple WDM channels, LDs from different materials are used so that different copies of the SMDs can emit light of different wavelengths for communication. In this work, ten devices with ten wavelengths have been made which include three blue LDs (405 nm, 450 nm, 455 nm) and seven infrared LDs (850 nm, 900 nm, 905 nm, 940 nm, 955 nm, 980 nm, 1064 nm). The light beams from illumination and communication LDs form an overlapped emission from the phosphor reflector. Compared to conventional LED-based light sources, the presented SMD laser source offers much higher optical power and a dramatic increase in modulation bandwidth for LiFi.

IV. High Speed LiFi Transmission With a Single Channel

The multi-channel LiFi transmission is composed of a number of single links with various wavelengths in parallel, which share a similar system deign. In this section, the details of experimental design and the performance of a single LiFi link are presented. A block diagram of a single link LiFi system is shown in Fig. 3. The optical link system is composed of software and hardware parts. The transmitter hardware includes a high-speed arbitary waveform generator (AWG), Keysight M8195 A, to convert digital signals to high-speed analogue waveform, a power amplifier, Mini-Circuit ZHL-42W+, to boost the modulated alternating current (AC) signal, a bias-T, Mini-Circuit ZFBT-282-1.5A+, to combine the direct current (DC)-bias and AC signal, and the SMD light source that was presented in Section III to convert the electrical signal to an optical signal. The light from both LDs is coupled into an optical fibre for delivery to a launch optic. The receiver hardware is composed of a collimating lens to focus the detected light, a positive-intrinsic-negative (PIN) detector, Femto receiver HSA-X-S-1G4-SI, to convert the optical signal to a photocurrent signal and a high-speed oscilloscope, Keysight MXR608 A, to convert analogue waveforms back to digital signals.

Various communication signal processing, such as modulation, channel estimation and channel equalisation, are conducted on the software side by a personal computer (PC). The spectral efficient DC-biased optical (DCO)-OFDM with quadrature amplitude modulation (QAM) modulations are implemented in this work [32]. On the transmitter side, random information binary bits are generated and modulated as QAM symbols $X[k]$. To guarantee the time-domain signal to be real-valued, the frequency-domain QAM symbols need to fulfil the Hermitian symmetry, which requires $X[k] = X^*[K-k]$, where $k = 0, 1, \ldots, K-1$, K is the length of the OFDM symbol and $\{\cdot\}^*$ is the complex conjugate operator. This also implies that there are $K/2-1$ information carrying symbols in each OFDM frame. Then, the frequency-domain signal can be converted to a time-domain signal via an inverse fast Fourier transform (IFFT) operation [33]:

$$x[n] = \frac{1}{\sqrt{K}} \sum_{k=0}^{K-1} X[k] \exp\left(\frac{2\pi j n k}{K}\right). \tag{1}$$

A cyclic prefix (CP) is added at the beginning of each OFDM frame to deal with the non-flat channel and the interference between adjacent OFDM frames. Pulse shaping has been also used to make the digital signal band-limited:

$$x(t) = \sum_{n=0}^{K-1} x[n] p\left(t - n T_{\mathrm{s}}\right), \tag{2}$$

where $p(t)$ is defined as an root-square raised cosine (RRC) signal pulse and T_{s} is the symbol period. The high amplitude samples of the time-domain signals are clipped to avoid excessive high peak-to-average power ratio (PAPR) of the OFDM signal:

$$\hat{x}(t) = \begin{cases} \sigma_{\mathrm{x}}\kappa & : x(t) \geq \sigma_{\mathrm{x}}\kappa \\ x(t) & : -\sigma_{\mathrm{x}}\kappa < x(t) < \sigma_{\mathrm{x}}\kappa \\ -\sigma_{\mathrm{x}}\kappa & : x(t) \leq -\sigma_{\mathrm{x}}\kappa \end{cases}, \tag{3}$$

where σ_{x} is the standard deviation of $x(t)$ and κ is the clipping level. After the signal clipping, the signal is forwarded to the AWG for data transmission.

At the receiver side, the received signal from the scope $y(t)$ is forwarded to a matched filter which downsample the signal to

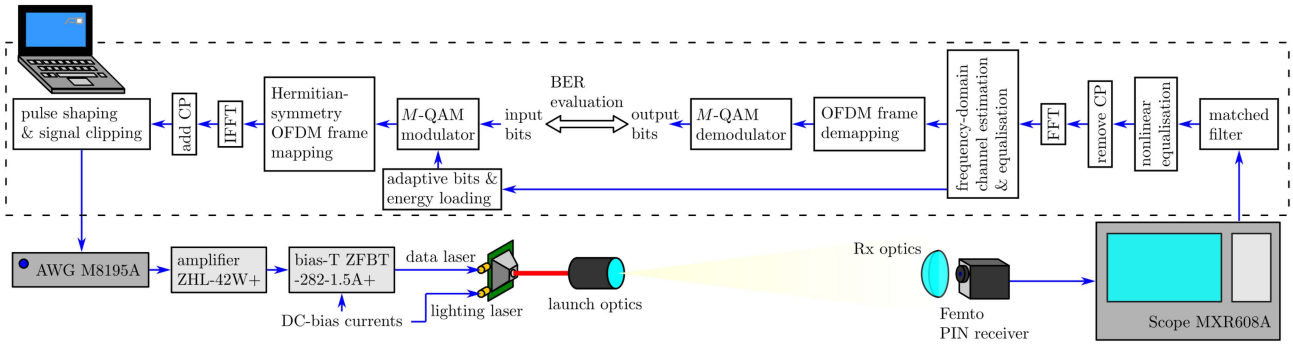

Fig. 3. Block diagram of a single link LiFi system.

the symbol rate and removes the out-of-band noise:

$$y[n] = \{y \otimes p\}(t = nT_{\mathrm{s}}), \tag{4}$$

where $\otimes$ is the convolution operator. The SMD laser source has a very low input impedance (a few ohms) compared to the bias-T output impedance (50 Ω). Consequently, it causes a severe impedance mismatch and signal reflections within the cable in-between. In addition, measurements showing significant nonlinearity exist in the optical link. In order to address these issues, cable length between bias-T and the SMD laser is minimised to avoid interference from the reflected signal in low frequency region. Furthermore, a Volterra nonlinear equaliser is implemented at the receiver side after the matched filter, as shown in Fig. 3. Therefore, the output of the nonlinear Volterra equaliser can be written as [34]:

$$z[n] = \sum_{Q=1}^{Q_{\max}} \sum_{l_1=-L}^{L} \cdots \sum_{l_q=-L}^{L} \cdots \sum_{l_Q=-L}^{L} w^{Q}_{l_1,\ldots,l_q,\ldots,l_Q} \times \prod_{q=1}^{Q} y[n-l_q], \tag{5}$$

where Q is defined as the polynomial order and L is half of the tap delay line, which corresponds to $2L+1$ taps in total. A maximum filter order of $Q_{\max}$ is considered. The conventional Volterra nonlinear equaliser has a very high complexity when $Q_{\max}$ is large. In many studies, simplified high-order nonlinear equalisers, such as memoryless polynomial, have been used to reduce the system complexity. In this work, we consider a modified Volterra nonlinear equaliser:

$$z[n] = \sum_{Q=1}^{Q_{\max}} \sum_{l_1=-L_Q}^{L_Q} \cdots \sum_{l_q=-L_Q, |l_q-l_1|\le D_Q}^{L_Q} \cdots \sum_{l_Q=-L_Q, |l_Q-l_1|\le D_Q}^{L_Q} w^{Q}_{l_1,\ldots,l_q,\ldots,l_Q} \prod_{q=1}^{Q} y[n-l_q], \tag{6}$$

where terms of different orders depend on tap delay lines of different lengths. The tap delay line length of the Qth order is L_Q. The high order terms with products of samples with differences in delay greater than D_Q are omitted. These changes can greatly reduce the number of high-order terms so that the computation complexity can be controlled. The modified nonlinear equaliser is trained by pilot symbols via a recursive least square (RLS) algorithm defined in Algorithm 1, where $\mathbf{y}_n$ is the nonlinear equalizer input polynomial vector:

Algorithm 1: Volterra Equaliser RLS Algorithm [34].

Initialisation: $\mathbf{S}_{L_{\max}-1} = \frac{1}{\sigma_x^2}\mathbf{I}_{N_{\mathrm{nl}}}$, $\mathbf{w}_{L_{\max}-1} = \mathbf{0}_{N_{\mathrm{nl}}\times 1}$

for $n = L_{\max}, \cdots, L_{\max} + N_{\mathrm{iter}}$ **do**

  Updata tap delay line and $\mathbf{y}_n$

  $e[n] = x[n] - \mathbf{y}_n^{\mathrm{T}}\mathbf{w}_{n-1}$

  $\mathbf{s}_n = \mathbf{S}_{n-1}\mathbf{y}_n$

  $\mathbf{S}_n = \frac{1}{\beta}\left(\mathbf{S}_{n-1} - \frac{\mathbf{s}_n\mathbf{s}_n^{\mathrm{T}}}{\beta+\mathbf{s}_n^{\mathrm{T}}\mathbf{y}_n}\right)$ $\mathbf{w}_n = \mathbf{w}_{n-1} + e[n]\mathbf{S}_n\mathbf{s}_n$

end

return $\mathbf{w}_{L_{\max}+N_{\mathrm{iter}}}$

$$\begin{aligned}\mathbf{y}_n = \Big[& y[n+L_1], \ldots, y[n-L_1], \ldots, y^2[n+L_2], \ldots, \\ & y[n-l_1]y[n-l_2], \ldots, y^2[n-L_2], \ldots, y^Q[n+L_Q], \ldots, \\ & \prod_{q=1}^{Q} y[n-l_q], \ldots, y^Q[n-L_Q], \ldots, y^{Q_{\max}}[n+L_{Q_{\max}}], \ldots, \\ & \prod_{q=1}^{Q_{\max}} y[n-l_q], \ldots, y^{Q_{\max}}[n-L_{Q_{\max}}] \Big]^{\mathrm{T}}, \end{aligned} \tag{7}$$

which include N_{nl} terms and $\mathbf{w}_n$ is the weight vector:

$$\begin{aligned}\mathbf{w}_n = \Big[& w^1_{-L_1}, \ldots, w^1_{L_1}, \ldots, w^2_{-L_2,-L_2}, \ldots, w^2_{l_1,l_2}, \ldots, \\ & w^2_{L_2,L_2}, \ldots, w^Q_{-L_Q,\ldots,-L_Q}, \ldots, w^Q_{l_1,\ldots,l_Q}, \ldots, w^Q_{L_Q,\ldots,L_Q}, \\ & \cdots, w^{Q_{\max}}_{-L_{Q_{\max}},\ldots,-L_{Q_{\max}}}, \ldots, w^{Q_{\max}}_{l_1,\ldots,l_{Q_{\max}}}, \ldots, \\ & w^{Q_{\max}}_{L_{Q_{\max}},\ldots,L_{Q_{\max}}} \Big]^{\mathrm{T}}. \end{aligned} \tag{8}$$

The time-domain OFDM signal after pulse shaping (Fig. 3) is used as the reference signal $x[n]$ in Algorithm 1. In this work, the nonlinear equaliser highest filter order $Q_{\max}$, number of

TABLE II
SYSTEM SETTING FOR 905 NM LD

Parameters	Values
AWG peak-to-peak voltage	140 mV
DC-bias current	1171 mA
Modulation bandwidth	2.67 GHz
Pulse shaping roll-off factor	0.1
FFT size	1024
CP length	20
Clipping level	3.2
Highest nonlinear equaliser order	5
Nonlinear equaliser number of taps for {2nd to 5th}	{16, 7, 3, 2}
Nonlinear equaliser largest delay difference {2nd to 5th}	{1, 0, 0, 0}

taps L_Q and the maximum delay difference D_Q are optimised to achieve the highest data rate. Nonlinear equalisers of up to 5th order have been evaluated. In addition, the number of terms with different filter order is not greater than 50 so that the equaliser complexity is controlled in a feasible region. The redundant CP is removed and followed by an fast Fourier transform (FFT) operation, which convert the time-domain signal to frequency-domain:

$$Y[k] = \frac{1}{\sqrt{K}} \sum_{n=0}^{K-1} z[n] \exp\left(\frac{-2\pi jnk}{K}\right). \tag{9}$$

A one-tap equalisation is executed to retrieve the transmitted QAM symbols:

$$\tilde{X}[k] = Y[k]/H[k], \tag{10}$$

where $H[k]$ is the channel transfer function which can be estimated by sending pilot 4-QAM symbols with unit variance. Finally, the equalised symbols $\tilde{X}[k]$ are decoded and compared with the original binary bits for bit error rate (BER) calculation.

In the modulation and demodulation process, the variance of the QAM symbols and the constellation order are adaptively selected according to the channel estimation information so that the available modulation bandwidth can be fully utilized and the achievable data rate can be maximised. In this work, the Hughes-Hartogs (HH)-based adaptive bit and energy loading algorithm has been adopted, which has been widely used in many multi-carrier transmission systems [35].

In this work, SMD laser sources with ten different wavelengths for the communication LD have been used. The communication channels corresponding to each wavelength shows a different characteristic. In this section, the performance results of the 905 nm LD is presented. The used system settings are listed in Table II, where the AWG peak-to-peak voltage and the DC-bias current are carefully selected so that the average signal-to-noise ratio (SNR) across the modulation bandwidth is maximised. Note that the selection of modulation bandwidth can be greater than the channel bandwidth as the adaptive bit and energy loading function can avoid to load transmission resource to those subcarriers with very low SNR.

The results of SNR at various frequencies with a 905 nm SMD laser are shown in Fig. 4. It can be observed that the achievable SNRs below 1 GHz are above 20 dB, but SNRs at a higher frequency drops significantly. This is due to a number of factors: 1. The used PIN receiver has a 3-dB bandwidth of 1.4 GHz and

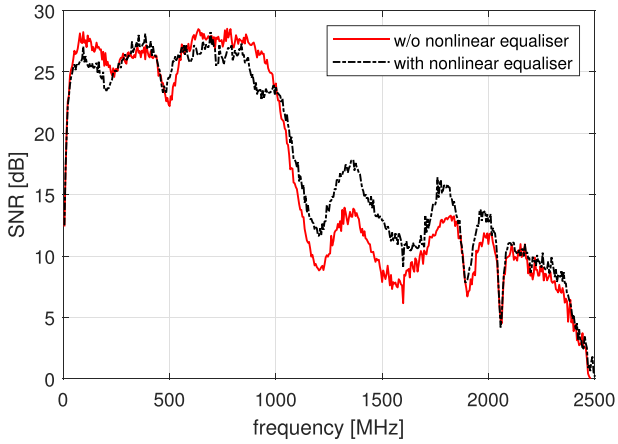

Fig. 4. Estimated SNR of LiFi link with 905 nm LD on subcarriers of various frequencies with and without nonlinear equaliser.

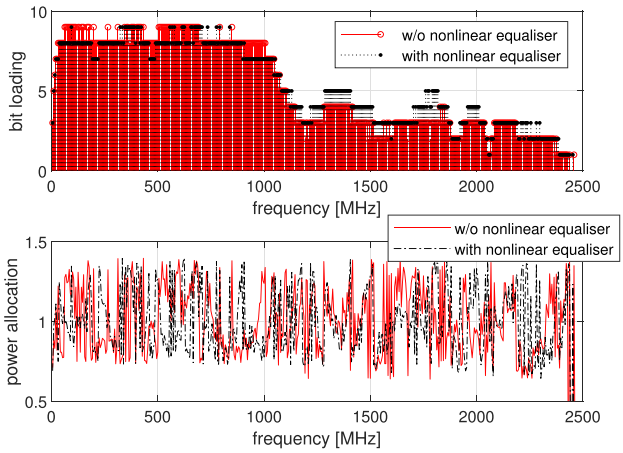

Fig. 5. An example of the adaptive bit (top figure) and energy (bottom figure) loading results.

the responses beyond this frequency are severely degraded; 2. The system nonlinearity limits the achievable SNRs at a high frequency; 3. The SNR is affected by the interference caused by signal reflections due to impedance mismatch. Despite the severe performance degradation at a high frequency, the maximum usable bandwidth is up to 2.5 GHz. It can also be observed that the link with nonlinear equaliser achieves higher SNRs on some subcarriers, especially for high frequency subcarriers. However, it generally worsen the SNR at very low frequency region. Overall, the nonlinear equaliser brings a boost to the high speed optical link quality. The high data rate transmission with up to 3 m was achieved with a single channel.

Based on the estimated channel and SNRs shown in Fig. 4, the adaptive bit and energy loading algorithm allocate different amounts of energy and numbers of bits to each subcarrier. One of the loading results is demonstrated in Fig. 5. It can be observed that the number of bits is highly related to the estimated SNR. The energy loading adjust the SNR to match the level that is just sufficient to transmit the allocated bit at the targeted BER. The transmitted and received QAM symbols of

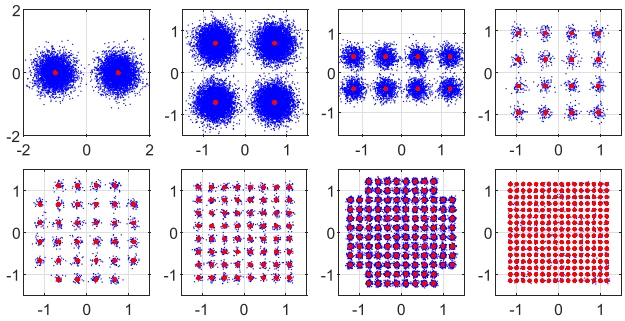

Fig. 6. Transmitted (red dots) and received (blue dots) QAM symbols of different modulation orders ($M = 2, 4, 8, 16, 32, 64, 128, 256, 512$).

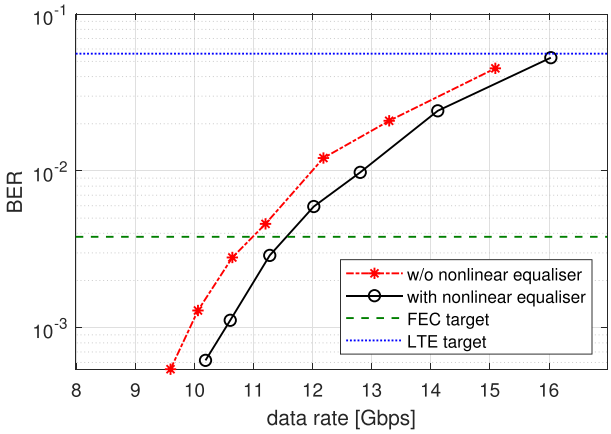

Fig. 7. BER results against achievable data rate of LiFi link with 905 nm LD.

different modulation orders are demonstrated in Fig. 6, which demonstrated the successful equalisations of the symbols.

The results of resultant BER against various achieved data rate are shown in Fig. 7. It can be observed that the achievable data rate by the system with a nonlinear equaliser is slightly higher than that without a nonlinear equaliser, which is consistent with the SNR results shown in Fig. 4. In this study, a BER threshold of 5.6×10^{-2} is considered. This BER threshold has been used in Long-Term Evolution (LTE), and it has been shown that with soft decision decoding and 3% to 5% overhead, such a BER target is acceptable to reduce the final BER below 1×10^{-6} [36]. By considering such a BER target, the achievable date rate can reach regions above 14 Gbps with 905 nm SMD laser source.

V. Over 100 Gbps LiFi Transmission With Parallel Channels

In Section IV, the details about the LiFi system design for a single channel are introduced. On top of the single link design, a LiFi transmission system with ten parallel channels are presented in this section. The block diagram of the multi-channel LiFi transmission system is shown in Fig. 8. With regards to hardware part, ten copies of amplifiers and bias-Ts in conjunction with three 4-channel AWGs are deployed to drive the SMD laser sources of different wavelengths. The output of the ten SMD laser sources are injected into a fibre bundle, which combines the optical signals and guides the light to a single launch optic. On the receiver side, an 2×5 array of PIN photodiode (PD) receivers are deployed. An optical filter with a 10 nm passband corresponds to each wavelength is mounted on each receiver to remove the crosstalk from other channels. Two 8-channel oscilloscopes are used to convert the photocurrent signals from ten receivers to digital signals. Therefore, the implemented system achieves parallel transmission via a WDM approach. Regarding the wavelengths of the LDs, there are seven infrared (IR) devices: 850 nm, 900 nm, 905 nm, 940 nm, 955 nm, 980 nm, 1064 nm and three blue devices. For the case of transmission via IR devices, the blue LD mounted on the same device should also be activated by a DC signal to provide white light illumination. For the case of transmission via blue devices, this is unnecessary as the communication LD provides white light illumination, as well. To ensure the considered optical setup is feasible, a simulation in Zemax Opticstudio has been conducted to estimate the received optical power after each receiver lens. The optical setup defined in the simulation is illustrated in Fig. 9(a). The simulation results show that the detected optical power after the receivers lens are in the range of a few to tens of mW, which is sufficient for reliable communication. An actual implementation of the optical system hardware is shown in Fig. 9(b).

With regards to software, the communication signal processing for each channel is identical to that introduced in Section IV but with different setting parameters. In addition, the communication signal processing for all channels are executed in parallel. Due to the a number of undesired factors, such as temperature, nonlinearity, channel estimation error, the achieved BER of each channel may deviate from the target level. Therefore, a simple adaptive algorithm is deployed to slightly adjust the bit loading solution so that the effective BER converges to the target after a few iterations. The setting parameters of different channels are listed in Table III. Except the FFT size, pulse shaping roll-off factor and CP length, the setting parameters are adjusted to the optimised values so that the resultant achievable data rates are maximised. It can be observed that the channels with blue LDs require generally a high peak-to-peak voltage to overcome the stronger background noise in the blue spectrum region. Compared to channels with blue LDs, channels with IR LDs use a higher bias current and a wider modulation bandwidth. Note that nonlinear equalisers are not used on five out of the ten channels, as shown in the 5th row of Table III. This is because the use of a nonlinear equaliser brings negligible SNR improvement on these channels.

The SNR and BER results of all channels are shown in Figs. 10 and 11, respectively. It can be observed that the performance of different channels varies significantly due to the characteristics of each LD. In those links, there is sufficient optical power received by optical detectors owing to the short transmission range. Consequently, the optical link performance is mainly limited by nonlinear distortion at electrical-to-optical conversion in the laser. To mitigate this nonlinear distortion, relatively smaller signal amplitudes (peak-to-peak voltage of the AC signal) were used in the multi-channel LiFi transmission which were sufficient for the short communication distance, as

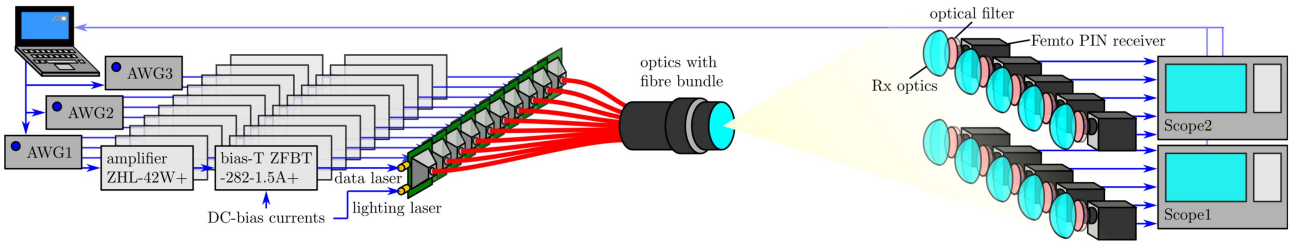

Fig. 8. Block diagram of LiFi transmission system with multiple parallel channels.

TABLE III
SYSTEM SETTING AND RESULTS FOR LIFI TRANSMISSION WITH PARALLEL CHANNELS

Wavelengths [nm]	405	450	455	850	900	905	940	955	980	1064	Aggregate
AWG peak-to-peak voltage [mV]	280	450	320	200	100	140	140	140	130	175	
DC-bias current [mA]	930	1000	1050	1000	1100	1171	1450	1450	1300	1050	
Modulation bandwidth [GHz]	1.33	1.6	1.6	2.67	3	2.67	2.67	2.67	2.67	3	
Clipping level	3.4	3.2	3.3	3.2	3.9	3.2	3.2	3.2	3.2	3.4	
Highest nonlinear equaliser order	5	0	3	0	3	5	0	0	0	3	
Data rate [Gbps]	4.62	7.44	6.97	9.65	14.2	14.48	11.4	12	11.4	13.2	105.36
BER	0.015	0.016	0.014	0.016	0.015	0.028	0.009	0.007	0.007	0.018	0.0148

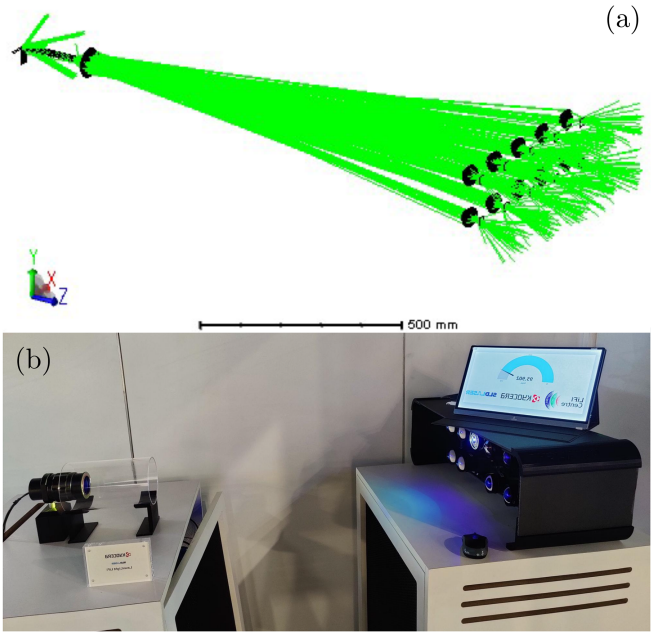

Fig. 9. Optical setup of the LiFi transmission system with ten parallel channels. (a) Zemax opticstudio. (b) Actual implementation.

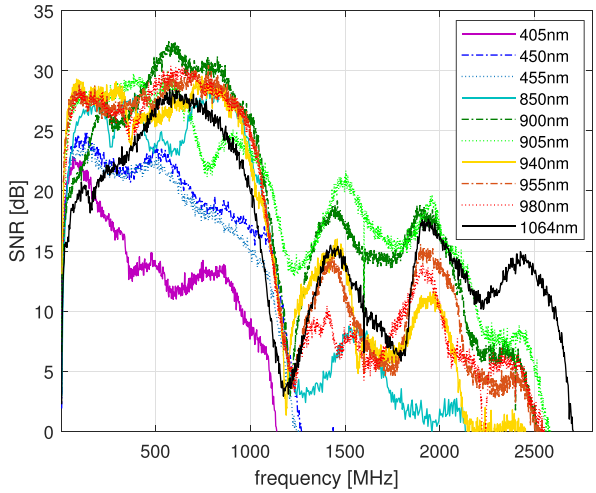

Fig. 10. SNR against frequency of LiFi transmission with multiple parallel channels.

shown in Table III. Since the noise level is lower and the laser bandwidths are wider on the IR channels compared to those on the visible light channels, a much lower signal amplitude can be used on the IR channels to mitigate nonlinear distortion. Consequently, the peak SNRs and bandwidths on the IR channels are higher than those on the visible light channels, as shown in Fig 10. The three blue light channels achieve slightly worse link quality, where the usable bandwidths are above 1 GHz but lower than 1.5 GHz. The achievable SNRs are in the range of 10 to 25 dB. Therefore, the achievable data rates are below 10 Gbps. In particular, the achievable data rate by 405 nm LD is below 6 Gbps. In contrast, performance of links with IR LDs are considerably superior, which generally exhibits a bandwidth of at least 2 GHz. In particular, the case with a 1064 nm laser uses a different PIN PD receiver (HSA-X-S-2G-IN) with a wider 3-dB bandwidth of 2 GHz, which boosts the total usable bandwidth to about 2.7 GHz. In addition, the achievable SNRs by IR links at low frequency region (below 1 GHz) are in the range of 20 to 30 dB, while the achievable SNRs at the high frequency region (above 1 GHz) are up to 20 dB, which lead to achievable data rates above 10 Gbps. The achievable data rates of the ten parallel channels are concluded in Table III, which shows that the aggregated data rate of above 100 Gbps is achievable with a BER lower than the LTE BER target.

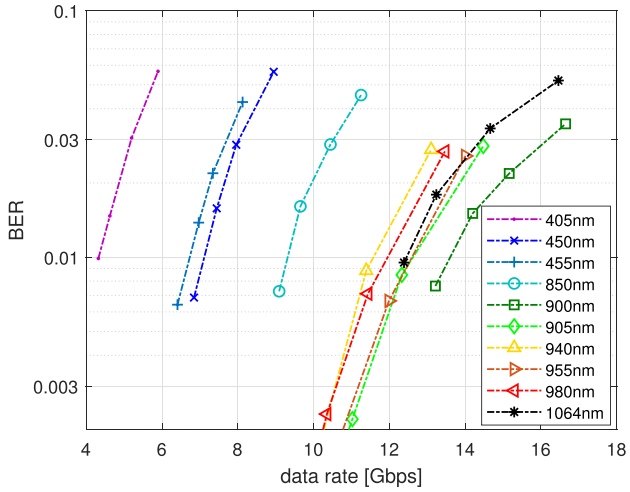

Fig. 11. BER against achievable data rate of LiFi transmission with multiple parallel channels.

VI. Long-Range LiFi Transmission

As discussed in Section II, the short range ultra high speed WDM LiFi system will be useful in many indoor use cases. In addition, long-range high speed LiFi transmission systems will also be attractive in vehicular communication and backhaul link use cases. Therefore, we showcase a long-range LiFi transmission based on the SMD laser source over 500 m in this section. The optical setup of the LiFi system is illustrated in Fig. 12. On the transmitter side, a Newtonian telescope, Orion StarBlast 4.5 Astro Reflector Telescope, is used to launch the light. The telescope has a focal length of 450 mm, a focal ratio of $f/4$ and an aperture diameter of 113 mm. The SMD laser device is mounted on the top of the telescope eyepiece with a downward orientation. The SMD laser source emitting spot is positioned on the focal point of a 1-inch aspherical condenser lens with a numerical aperture (NA) of 0.79 (lens 1), which is used to capture most of the emitted light from the SMD laser device. A second plano-convex Lens (lens 2) is used to shape the light beam with the same focal ratio of the telescope. The focal point of the second lens and focal point of the telescope are collocated. Therefore, the output light of the telescope has a plane wavefront. Note that the secondary mirror of the telescope blocks some of the emitted light which is inevitable with a Newtonian telescope-based optical design. On the receiver side, a 75 mm diameter aspherical lens, Thorlab ACL7560 U is used to capture the light after 500 m propagation distance. To compensate for the severe geometric loss over the long propagation distance, a high-gain avalanche photodiode (APD) receiver, Hamamatsu C5658, is used to detect the captured light by the receiver lens. This APD receiver has a 3-dB bandwidth of 1 GHz and an APD gain of 100.

The long-range measurement was conducted at the University of Strathclyde Stepps Playing Fields sport centre. The transmitter and the receiver are positioned at the two ends of the sport centre, as shown in the Google earth screenshot in Fig. 13. It can be seen that the measured separation between the transmitter and the receiver on Google earth was a little more than 500 m. Note that the altitudes at different locations in the sport centre vary slightly. The transmitter and the receivers are located at the high grounds. Therefore, the trees and other objects at the low ground were not obstructing the LOS path of the link.

TABLE IV
System Setting and Results for LiFi Transmission Over 500 m

Wavelengths [nm]	450	905	Aggregate
AWG peak-to-peak voltage [mV]	700	450	
DC-bias current [mA]	850	850	
Modulation bandwidth [GHz]	1.33	1.14	
Data rate [Gbps]	2.41	2.43	4.84
BER	0.0028	0.0035	0.0032

In order to justify that the considered optical setup is feasible to deliver long-range wireless communication, a simulation in Zemax Opticstudio has been conducted. The optical setup is defined based on the specification shown in Fig. 12 and a 5 m-by-5 m detector is defined at the receiver plane to capture the light pattern. The computer-aided design (CAD) model of the optical setup is illustrated in Fig. 14(a). The simulation result in terms of incoherent irradiance is shown in Fig. 14(b), where the light pattern at the receiver plane is about 3 m wide and about 2 m high. The actual light pattern has been captured by a camera during the night time, as shown in Fig. 14(c), which shows a close match to the simulation result.

The system parameter settings are summarised in Table IV. In this experiment, a single SMD laser source is used, which is capable of emitting light in two wavelengths: 450 nm and 905 nm. Due to the significant geometric loss, the detectable optical power is much less than the short range scenario. Consequently, the performance of the optical links are limited by receiver noise. Therefore, higher peak-to-peak voltages of 700 mV and 450 mV are used for 450 nm and 905 nm channels, respectively. In addition, due to the restricted cooling methods in the outdoor scenario (a 5 cm-by-5 cm cooling fan), the bias current has to be limited to 850 mA. As shown in Figs. 4 and 10, the links with the SMD laser sources exhibit higher SNRs at low frequency regime (< 1 GHz) and lower SNRs at the high frequency regime (> 1 GHz). Due to the lower received optical power, the overall signal quality is much worse than in the short-range scenario. Consequently, reliable transmission over high frequency subcarriers are not possible. Therefore, modulation bandwidth of 1.33 GHz and 1.14 GHz are used on 450 nm and 905 nm channels, respectively. Since the limiting factor is receiver noise, nonlinear equaliser is not used, which cannot effectively improve the performance.

The long-range communication performance is concluded in Figs. 15 and 16. Compared to the short-range scenarios, the received optical power levels are much lower due to the geometric loss, which makes the system performance limited by receiver noise. In this scenario, higher signal amplitudes have to be used to overcome the receiver noise, as shown in Table IV, but this leads to more severe nonlinear distortion at the transmitter end. Under such an operation condition, the 905 nm IR channel no longer shows superiority to the visible light 450 nm channel in terms of peak SNR. The resultant SNRs decrease to a range of

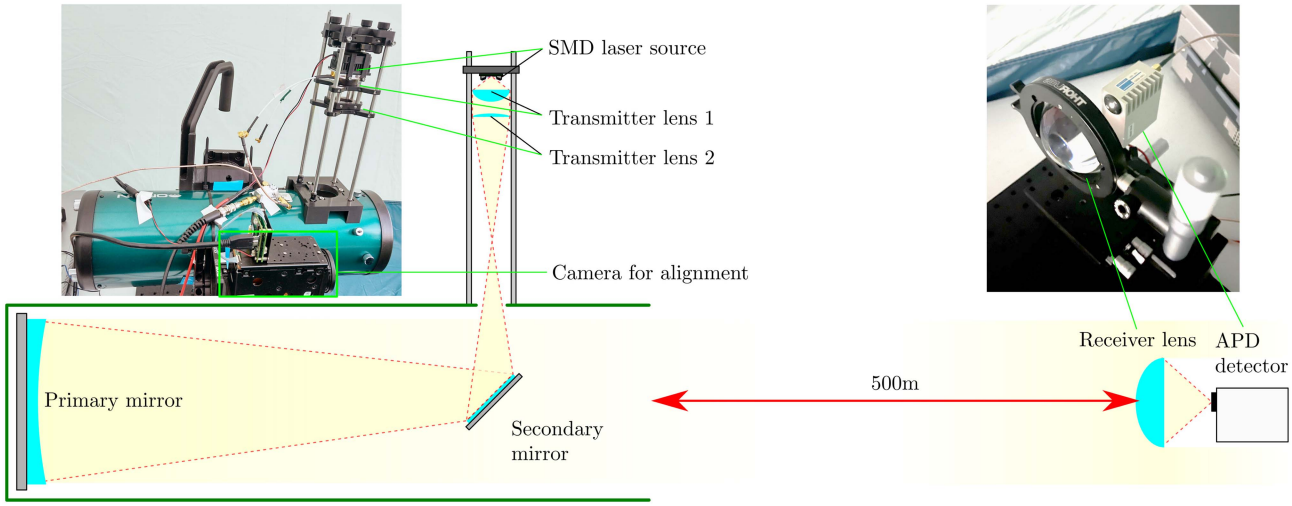

Fig. 12. Setup of the transmitter and the receiver for long-range LiFi link.

Fig. 13. long-range LiFi transmission measurement site on Google earth screenshot.

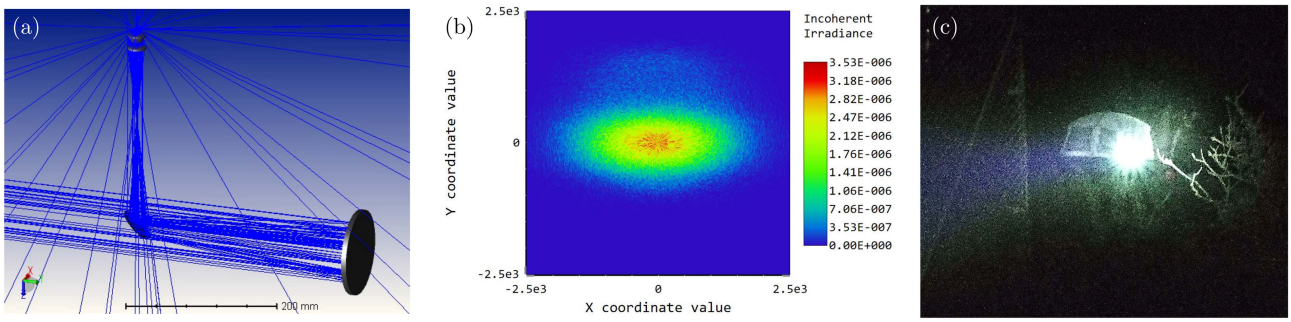

Fig. 14. (a) Zemax opticstudio simulation setup. (b) Incoherent irradiance light pattern at receiver plane obtained in simulation. (c) Actual light pattern at receiver plane taken by a camera.

5 to 15 dB, as shown in Fig. 15. In the case of 450 nm channel, the usable modulation bandwidth is up to 1.2 GHz. The estimated SNR is around 10 dB over the used modulation bandwidth. In the case of the 905 nm channel, a slightly narrower modulation bandwidth of 1.05 GHz has been achieved. However, for the subcarriers in the frequency range of 400 MHz to 800 MHz, the achievable SNRs are higher than those on the 450 nm channel by 2–3 dB. The bandwidth of the 905 nm channel in the long-range scenario is narrower than that in the short-range scenario. This is mainly due to the use of different receiver detectors. Wideband PIN receivers are used in the short-range scenarios to boost the modulation bandwidth while a high gain APD receiver has been used in the long-range scenario to compensate for the low received optical power. The APD receiver has a narrow 3-dB bandwidth of 1 GHz.

In terms of BER against achievable data rate, the performance of links with the two channels is similar, as shown in Fig. 16. The 450 nm channel can achieve a data rate of 2.41 Gbps with a

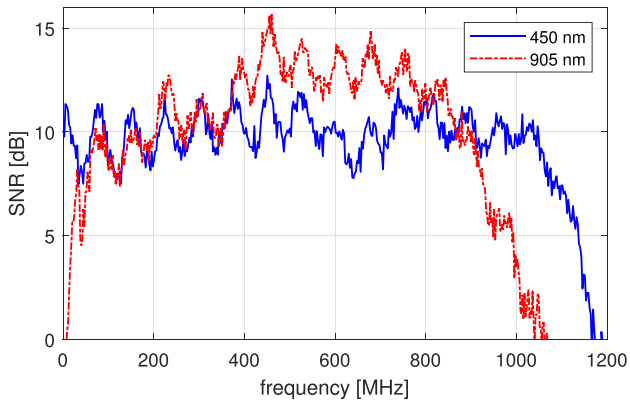

Fig. 15. Estimated SNR against frequency in the long-range LiFi link.

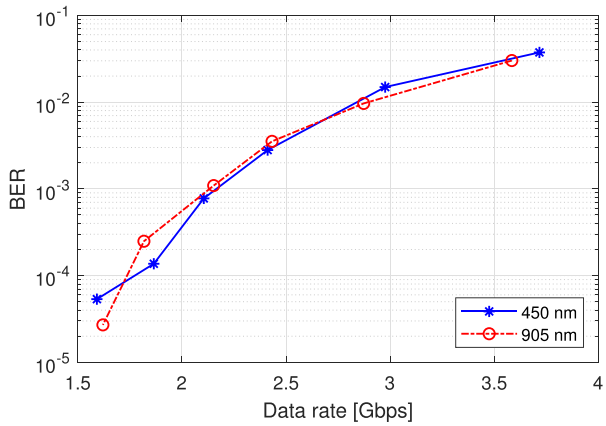

Fig. 16. BER against data rate in the long-range LiFi link.

BER of 0.0028 and the 905 nm channel can achieve a data rate of 2.43 Gbps with a BER of 0.0035. Therefore, the aggregate data rate is about 4.84 Gbps with an effective BER of 0.0032, which is lower than the forward error correction (FEC) target. This long-range LiFi link demonstrate that the SMD laser device can be used to achieve multi-Gbps data rate LiFi transmission in a long-range distance of at least 500 m.

The LiFi transmissions in the long-range scenarios are affected by various atmospheric effects [37]. Firstly, the light is attenuated by small molecules in the air due to absorption or scattering. In addition, weather conditions such as rain, fog and snow may cause more severe absorption and scattering, which leads to significant light attenuation. Finally, the atmospheric turbulence caused by variations in temperature and pressure leads to scintillation effects on the optical link. However, during the long-range LiFi transmission measurement period, no significant atmospheric effects have been observed. This is because of the following reasons:

- The impacts of atmospheric effects become more significant when the link distance increases. A link distance of 500 m is not enough for noticeable atmospheric effects. Furthermore, the experiments were conducted on clear days. We might have observed more obvious performance degradation if there was fog or rain during the measurements.
- A large receiver aperture of 75 mm in diameter has been used, which exhibits a spatial averaging effect and mitigates the scintillation effect.
- For the optical link on the 450 nm channel, no optical filter has been used. Therefore, propagated light has a wide optical spectrum (appear to be white). Consequently, the receiver can detect light from multiple wavelength components. Therefore, the atmospheric effects can be further mitigated due to this wavelength diversity.

In future research, we will extend the link distance of the long-range LiFi system and investigate the impacts of atmospheric effects on the LiFi system performance.

VII. Conclusion

In this paper, we have discussed the potential use cases of laser-based LiFi systems. We have demonstrated a LiFi WDM system based on ten SMD laser sources achieving over 100 Gbps data rate and a multi-Gbps long-range LiFi transmission over a distance of 500 m. In particular, we have demonstrated the use of a nonlinear equaliser to improve transmission channel quality. The experimental transmission performance in terms of SNR, BER and achievable data rates are presented. The demonstrated system proves that it is possible to scale the transmission capacity of the LiFi system by using multiple SMD laser sources of different wavelengths. In addition, it is also possible to utilise the high optical power feature of the SMD laser source to establish optical links over long distances.

References

[1] H. Haas et al., "Why optical wireless communications is ready for 6G," in *Proc. IEEE Eur. Conf. Opt. Commun.*, 2023, pp. 1594–1597.
[2] M. Barnoski, *Fundamentals of Optical Fiber Communications*. Amsterdam, The Netherlands: Elsevier, 2012.
[3] R. Roriz, J. Cabral, and T. Gomes, "Automotive LiDAR technology: A survey," *IEEE Trans. Intell. Transp. Syst.*, vol. 23, no. 7, pp. 6282–6297, Jul. 2022.
[4] I. Ichimura, F. Maeda, K. Osato, K. Yamamoto, and Y. Kasami, "Optical disk recording using a GaN blue-violet laser diode," *Japanese J. Appl. Phys.*, vol. 39, no. 2B, pp. 937–942, Feb. 2000, doi: 10.1143/jjap.39.937.
[5] H.-A. Chen, J.-W. Pan, and Z.-P. Yang, "Speckle reduction using deformable mirrors with diffusers in a laser pico-projector," *Opt. Exp.*, vol. 25, no. 15, pp. 18140–18151, Jul. 2017. [Online]. Available: http://opg.optica.org/oe/abstract.cfm?URI=oe-25-15-18140
[6] N. Trivellin et al., "Laser-based lighting: Experimental analysis and perspectives," *Materials*, vol. 10, no. 10, 2017, Art. no. 1166. [Online]. Available: https://www.mdpi.com/1996-1944/10/10/1166
[7] J. Y. Tsao et al., "Toward smart and ultra-efficient solid-state lighting," *Adv. Opt. Mater.*, vol. 2, no. 9, pp. 809–836, 2014.
[8] K. Hanna, "Kyocera SLD laser introduces high power blue laser diode product line for industrial, biomedical, defense and display applications," Business wire, Jan. 2023. [Online]. Available: https://www.businesswire.com/news/home/20230131005481/en/KYOCERA-SLD-Laser-Introduces-High-Power-Blue-Laser-Diode-Product-Line-for-Industrial-Biomedical-Defense-and-Display-Applications
[9] H. Haas, L. Yin, Y. Wang, and C. Chen, "What is LiFi?," *J. Lightw. Technol.*, vol. 34, no. 6, pp. 1533–1544, Mar. 2016.
[10] M. Shehata, Y. Wang, J. He, S. Kandeepan, and K. Wang, "Optical and terahertz wireless technologies: The race to 6G communications," *IEEE Wireless Commun.*, vol. 30, no. 5, pp. 10–18, Oct. 2023.
[11] D. Moltchanov, E. Sopin, V. Begishev, A. Samuylov, Y. Koucheryavy, and K. Samouylov, "A tutorial on mathematical modeling of 5G/6G millimeter wave and terahertz cellular systems," *IEEE Commun. Surveys Tuts.*, vol. 24, no. 2, pp. 1072–1116, Secondquarter 2022.

[12] H.-J. Song and N. Lee, "Terahertz communications: Challenges in the next decade," *IEEE Trans. Terahertz Sci. Technol.*, vol. 12, no. 2, pp. 105–117, Mar. 2022.
[13] D. Tse and P. Viswanath, *Fundamentals of Wireless Communication*. New York, NY, USA: Cambridge Univ. Press, 2005.
[14] I. F. Akyildiz, C. Han, Z. Hu, S. Nie, and J. M. Jornet, "Terahertz band communication: An old problem revisited and research directions for the next decade," *IEEE Trans. Commun.*, vol. 70, no. 6, pp. 4250–4285, Jun. 2022.
[15] F. Taleb et al., "Propagation of THz radiation in air over a broad range of atmospheric temperature and humidity conditions," *Sci. Rep.*, vol. 13, no. 1, 2023, Art. no. 20782.
[16] M. D. Soltani et al., "Safety analysis for laser-based optical wireless communications: A tutorial," *Proc. IEEE*, vol. 110, no. 8, pp. 1045–1072, Aug. 2022.
[17] F. Tariq, M. R. A. Khandaker, K.-K. Wong, M. A. Imran, M. Bennis, and M. Debbah, "A speculative study on 6G," *IEEE Wireless Commun.*, vol. 27, no. 4, pp. 118–125, Aug. 2020.
[18] D. Karunatilaka, F. Zafar, V. Kalavally, and R. Parthiban, "LED based indoor visible light communications: State of the art," *IEEE Commun. Surv. Tuts.*, vol. 17, no. 3, pp. 1649–1678, Thirdquarter 2015.
[19] E. Xie et al., "Over 10 Gbps VLC for long-distance applications using a GaN-Based series-biased Micro-LED array," *IEEE Photon. Technol. Lett.*, vol. 32, no. 9, pp. 499–502, May 2020.
[20] C. Shen et al., "High-speed 405-nm superluminescent diode (SLD) with 807-MHz modulation bandwidth," *Opt. Exp.*, vol. 24, no. 18, pp. 20281–20286, Sep. 2016. [Online]. Available: http://opg.optica.org/oe/abstract.cfm?URI=oe-24-18-20281
[21] D. Tsonev, S. Videv, and H. Haas, "Towards a 100 Gb/s visible light wireless access network," *Opt. Exp.*, vol. 23, no. 2, pp. 1627–1637, 2015.
[22] C. Lee et al., "4 Gbps direct modulation of 450nm GaN laser for high-speed visible light communication," *Opt. Exp.*, vol. 23, no. 12, pp. 16232–16237, Jun. 2015. [Online]. Available: http://opg.optica.org/oe/abstract.cfm?URI=oe-23-12-16232
[23] C. Lee et al., "Dynamic characteristics of 410 nm semipolar $(20\bar{2}\bar{1})$ III-nitride laser diodes with a modulation bandwidth of over 5GHz," *Appl. Phys. Lett.*, vol. 109, no. 10, 2016, Art. no. 101104.
[24] Y.-C. Chi et al., "Phosphorous diffuser diverged blue laser diode for indoor lighting and communication," *Sci. Rep.*, vol. 5, no. 1, pp. 1–9, 2015.
[25] H. Chun, S. Rajbhandari, D. Tsonev, G. Faulkner, H. Haas, and D. O'Brien, "Visible light communication using laser diode based remote phosphor technique," in *Proc. IEEE Int. Conf. Commun. Workshop*, 2015, pp. 1392–1397.
[26] R. Kirrbach, M. Faulwaßer, M. Stephan, T. Schneider, and F. Deicke, "High power Eye-safe optical wireless gigabit link employing a freeform multipath lens," *IEEE Commun. Lett.*, vol. 26, no. 6, pp. 1343–1347, Jun. 2022.
[27] B. Janjua et al., "Going beyond 4 Gbps data rate by employing RGB laser diodes for visible light communication," *Opt. Exp.*, vol. 23, no. 14, pp. 18746–18753, Jul. 2015. [Online]. Available: http://opg.optica.org/oe/abstract.cfm?URI=oe-23-14-18746
[28] C. Lee et al., "26 Gbit/s LiFi system with laser-based white light transmitter," *J. Lightw. Technol.*, vol. 40, no. 5, pp. 1432–1439, Mar. 2022.
[29] E. Cuervo, K. Chintalapudi, and M. Kotaru, "Creating the perfect illusion: What will it take to create life-like virtual reality headsets?," in *Proc. 19th Int. Workshop Mobile Comput. Syst. Appl.*, 2018, pp. 7–12.
[30] C. Chen, D. A. Basnayaka, and H. Haas, "Downlink performance of optical attocell networks," *J. Lightw. Technol.*, vol. 34, no. 1, pp. 137–156, Jan. 2016.
[31] A.-M. Căilean and M. Dimian, "Current challenges for visible light communications usage in vehicle applications: A survey," *IEEE Commun. Surv. Tuts.*, vol. 19, no. 4, pp. 2681–2703, Fourthquarter 2017.
[32] X. Zhang, Z. Babar, P. Petropoulos, H. Haas, and L. Hanzo, "The evolution of optical OFDM," *IEEE Commun. Surv. Tuts.*, vol. 23, no. 3, pp. 1430–1457, Thirdquarter 2021.
[33] D. Tsonev, S. Sinanovic, and H. Haas, "Complete modeling of nonlinear distortion in OFDM-based optical wireless communication," *J. Lightw. Technol.*, vol. 31, no. 18, pp. 3064–3076, Sep. 2013.
[34] P. S. Diniz et al. *Adaptive Filtering*, vol. 4. Berlin, Germany: Springer, 1997.
[35] D. Hughes-Hartogs, "Ensemble modem structure for imperfect transmission media," U.S. Patent No. 4,679,227 (Jul. 1987); 4,731,816 (Mar. 1988); 4,833,706 (May 1989).
[36] B. P. Smith, A. Farhood, A. Hunt, F. R. Kschischang, and J. Lodge, "Staircase codes: FEC for 100 Gb/s OTN," *J. Lightw. Technol.*, vol. 30, no. 1, pp. 110–117, Jan. 2012.
[37] H. Kaushal, V. Jain, and S. Kar, *Free Space Optical Communication*, vol. 60. Berlin, Germany: Springer, 2017.